EUROPEAN JOURNAL OF PURE AND APPLIED MATHEMATICS
2026, Vol. 19, Issue 2, Article Number 6850
ISSN 1307-5543 – ejpam.com
Published by New York Business Global

Exploring Bladder Cancer Treatment Strategies Through a Discrete-Time Mathematical Model

Modhi Y. Alkharraz[1,2], Nadihah Wahi[1,*], N. M. A. Nik Long[1], Mahmoud A. Abdelaziz[3]

[1] *Department of Mathematics and Statistics, Faculty of Science, Universiti Putra Malaysia, 43400 UPM Serdang, Selangor, Malaysia*
[2] *Department of Mathematics, College of Science, Qassim University, P.O. Box 53, Buraydah 51921, Saudi Arabia*
[3] *Department of Mathematics, Faculty of Arts and Science, Najran University, Najran, Saudi Arabia*

Abstract. This paper investigates the dynamical behavior of a discrete-time bladder cancer–immune–virotherapy model. The model describes the interactions among uninfected tumor cells, infected tumor cells, free virus particles, tumor-specific immune cells, and virus-specific immune cells. The discrete formulation is obtained via Euler discretization of a biologically motivated continuous system, allowing the exploration of dynamical effects inherent to temporal discretization. We establish the existence and local stability conditions of biologically relevant equilibrium points and determine the basic reproduction number governing viral invasion. Furthermore, we analyze the occurrence of flip (period-doubling), fold, and Neimark–Sacker (N–S) bifurcations to characterize qualitative transitions in system dynamics. The results reveal distinct dynamical regimes induced by variations in the viral infection rate and time step size, including stable equilibria, sustained oscillations, and more complex discrete behaviors.
Numerical simulations support the analytical findings and illustrate how parameter changes influence tumor–virus–immune interactions. The study highlights the sensitivity of discrete tumor virotherapy models to parameter variation and emphasizes the role of discrete-time dynamics in shaping treatment-related outcomes.

2020 Mathematics Subject Classifications: 92C50, 37N25, 39A30

Key Words and Phrases: Cancer virotherapy, stability, dynamical systems, oncolytic viruses, tumor modeling, bifurcation analysis, discrete dynamics

*Corresponding Author.
DOI: https://doi.org/10.29020/nybg.ejpam.v19i2.6850

Email addresses: 26440@qu.edu.sa (M. Y. Alkharraz), nadihah@upm.edu.my (N. Wahi), nmasri@upm.edu.my (N. M. A. Nik Long), maabdelaziz@nu.edu.sa (M. A. Abdelaziz)

1. Introduction

Cancer remains one of the leading causes of morbidity and mortality worldwide despite continuous advances in medical research and treatment technologies [1, 2]. Among the various malignancies, bladder cancer constitutes a significant global health burden, characterized by high recurrence rates and considerable economic impact [3, 4]. The disease predominantly affects elderly individuals and exhibits a higher incidence in males. Conventional treatment strategies, including surgery, chemotherapy, radiotherapy, and Bacillus Calmette–Guérin (BCG) immunotherapy, have demonstrated clinical efficacy; however, these approaches are frequently associated with adverse side effects, recurrence, and treatment resistance [5, 6]. Consequently, the development of alternative and more targeted therapeutic strategies remains an important objective.

Oncolytic virotherapy has emerged as a promising approach in cancer treatment. This strategy employs genetically modified or naturally occurring viruses that selectively infect and lyse tumor cells while largely sparing normal tissues [7, 8]. Following infection, viral replication within cancer cells induces cell lysis and the release of new virions, which subsequently infect neighboring tumor cells. In addition to direct oncolysis, viral infection may stimulate anti-tumor immune responses, thereby enhancing therapeutic efficacy. However, the intricate interactions among tumor cells, virus particles, and multiple immune components complicate the prediction of treatment outcomes without a rigorous quantitative framework.

Mathematical modeling plays a central role in understanding tumor–virus–immune dynamics and assessing potential therapeutic strategies [9]. Numerous continuous-time models have been proposed to describe tumor growth under viral immunotherapy and immune activation, providing insight into threshold behavior, equilibrium stability, and treatment response. Nevertheless, discrete-time formulations may exhibit additional dynamical phenomena that are intrinsic to discrete systems, including period-doubling cascades, fold bifurcations, and Neimark–Sacker bifurcations, potentially leading to complex oscillatory or quasi-periodic behavior [10].

In this work, we propose and analyze a discrete-time bladder cancer–immune–virotherapy model obtained via Euler discretization of a biologically motivated continuous system. The model incorporates five interacting populations: uninfected tumor cells, infected tumor cells, free virus particles, tumor-specific immune cells, and virus-specific immune cells. The discrete framework enables a detailed investigation of stability switching and bifurcation structures as a function of key parameters, particularly the viral infection rate and the time step size.

The principal contribution of this study is the systematic characterization of local stability properties and codimension-one bifurcations in the discrete setting. Specifically, we establish conditions for the occurrence of flip (period-doubling), fold, and Neimark–Sacker bifurcations and analyze their dynamical implications. By combining algebraic stability criteria, bifurcation theory, and numerical simulations, we identify transitions between stable tumor control, sustained oscillatory tumor–immune interactions, and more complex discrete dynamical regimes.

Although continuous-time tumor–virus–immune interaction models have been extensively studied, the discrete-time formulation considered here introduces qualitatively distinct behaviors. In particular, discrete updating may generate flip and Neimark–Sacker bifurcations and invariant closed curves that do not arise in classical continuous frameworks. By systematically analyzing these discrete-specific transitions and their dependence on the time step size and infection parameters, this work extends existing tumor virotherapy models and highlights the dynamical consequences of temporal discretization.

The remainder of the paper is organized as follows. Section 2 formulates the bladder cancer model and presents the biological assumptions. Section 3 establishes the existence of equilibrium points. Local stability analysis is conducted in Section 4. Section 5 investigates the conditions for the existence of codimension-one bifurcations. Numerical simulations illustrating the theoretical findings are presented in Section 6. Finally, Section 7 concludes the paper with a discussion of the main results.

2. Mathematical model of bladder cancer

Figure 1 illustrates the schematic representation of the proposed mathematical model describing the interactions among cancer cells, oncolytic viruses, and adaptive immune responses. The model consists of five ordinary differential equations governing the dynamics of uninfected tumor cells, infected tumor cells, free virus particles, tumor-specific immune cells, and virus-specific immune cells. Tumor regression in this framework occurs through two principal mechanisms: (i) direct virus-induced lysis of infected cancer cells via replication-dependent processes and (ii) stimulation of anti-tumor immune responses targeting both infected and uninfected tumor cells [11]. The primary objectives of the continuous model are to investigate (1) the tumor response to oncolytic virus infection and (2) the influence of antitumor and antiviral adaptive immune responses on disease progression.

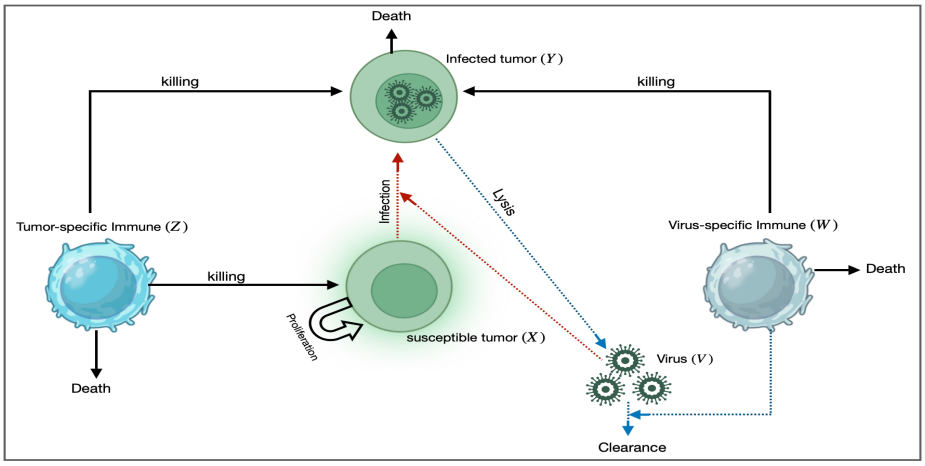

Figure 1: Interactions among cancer cells, viruses, and immune cells.

The formulation of the proposed model is based on the following biological assumptions:

(i) Uninfected tumor cells grow logistically toward a carrying capacity, reflecting environmental limitations. Infected tumor cells have a significantly shorter lifespan due to virus-induced lysis and therefore are not assumed to follow logistic growth [12].

(ii) In the present framework, virus-specific immune responses are assumed to be stimulated indirectly by infected tumor cells rather than free virus particles. This reflects the biological mechanism whereby infected cells present viral antigens and activate adaptive immune responses [13]. Consequently, proliferation of virus-specific immune cells is modeled through the interaction term $\gamma_5 yw$, while elimination of infected tumor cells mediated by these immune cells is represented by $\gamma_2 yw$.

(iii) Tumor-specific immune cells can recognize and eliminate both uninfected and infected tumor cells due to the expression of tumor-associated antigens [14].

(iv) No virus-specific immunity is assumed prior to virotherapy; thus, infected tumor cells and virus-specific immune cells initially start at zero.

(v) Upon lysis of an infected tumor cell, newly produced virions are released and infect neighboring uninfected tumor cells [15].

Under these assumptions, the continuous-time model is formulated as

$$\begin{aligned}
\frac{dx}{dt} &= rx\left(1-\frac{x}{k}\right) - \beta x\upsilon - \gamma_1 xz,\\
\frac{dy}{dt} &= \beta x\upsilon - \gamma_1 yz - \gamma_2 yw - \alpha y,\\
\frac{d\upsilon}{dt} &= b\alpha y - \theta\upsilon,\\
\frac{dz}{dt} &= \gamma_3 xz + \gamma_4 yz - \delta_1 z,\\
\frac{dw}{dt} &= \gamma_5 yw - \delta_2 w.
\end{aligned} \tag{1}$$

Here, $x(t)$ and $y(t)$ denote the populations of uninfected and infected tumor cells, respectively. The variable $\upsilon(t)$ represents free virus particles, $z(t)$ denotes tumor-specific immune cells, and $w(t)$ represents virus-specific immune cells. The biological interpretation of the model terms is summarized as follows:

- The term $rx\left(1-\frac{x}{k}\right)$ represents logistic growth of uninfected tumor cells, reflecting intrinsic proliferation and environmental carrying capacity constraints.
- The bilinear term $\beta x\upsilon$ models mass-action infection between free virus particles and susceptible tumor cells.
- Tumor-specific immune cells eliminate both uninfected and infected tumor cells through antigen recognition, represented by $\gamma_1 xz$ and $\gamma_1 yz$.

- Virus-specific immune responses are activated by infected tumor cells and contribute to infected cell clearance via $\gamma_2 yw$.
- Following infection, infected tumor cells lyse at rate α, releasing new virus particles at rate b, represented by the production term $b\alpha y$. Free virus particles decay at rate θ.
- Tumor-specific immune cells proliferate in response to tumor presence through $\gamma_3 xz$ and $\gamma_4 yz$, while virus-specific immune cells proliferate via $\gamma_5 yw$.
- Tumor-specific and virus-specific immune cells undergo natural death at rates δ_1 and δ_2, respectively.

All model parameters listed in Table 1 are assumed to be positive to ensure biological feasibility of the solutions.

Table 1: Biological Meaning of Model Parameters.

Parameter	**Biological Meaning**
r	Intrinsic growth rate of cancer cells.
k	Carrying capacity.
β	Viral infection rate.
α	Lysis rate of infected tumor cells.
b	Release rate of new free virions.
θ	Decay rate of virus particles.
δ_1	Natural death rate of tumor-specific immune cells.
δ_2	Natural death rate of virus-specific immune cells.
γ_1	Killing rate of cancer cells by tumor-specific immune cells.
γ_2	Clearance rate of infected tumor cells mediated by virus-specific immune cells.
γ_3	Proliferation rate of tumor-specific immune cells stimulated by uninfected cells.
γ_4	Proliferation rate of tumor-specific immune cells stimulated by infected cells.
γ_5	Proliferation rate of virus-specific immune cells stimulated by infected tumor cells.

To examine the model within a discrete-time framework, we apply the forward Euler discretization scheme to system (1). This discretization allows us to investigate dynamical behaviors that are intrinsic to discrete updates and that may not arise in the corresponding continuous-time formulation [16]. In particular, the discrete setting enables the analysis of stability switching and bifurcation phenomena associated with temporal sampling. Using the standard forward difference approximation

$$\frac{dx}{dt} \approx \frac{x_{n+1} - x_n}{h},$$

and proceeding analogously for the remaining state variables, we obtain the following discrete-time bladder cancer model:

$$\begin{aligned} x_{n+1} &= x_n + h\left[rx_n\left(1-\frac{x_n}{k}\right) - \beta x_n \upsilon_n - \gamma_1 x_n z_n\right], \\ y_{n+1} &= y_n + h\left[\beta x_n \upsilon_n - \gamma_1 y_n z_n - \gamma_2 y_n w_n - \alpha y_n\right], \\ \upsilon_{n+1} &= \upsilon_n + h\left[b\alpha y_n - \theta \upsilon_n\right], \\ z_{n+1} &= z_n + h\left[\gamma_3 x_n z_n + \gamma_4 y_n z_n - \delta_1 z_n\right], \\ w_{n+1} &= w_n + h\left[\gamma_5 y_n w_n - \delta_2 w_n\right]. \end{aligned} \tag{2}$$

Here, $h > 0$ denotes the discrete time step size. From a modeling perspective, h represents the temporal update interval of the system and may reflect observation frequency, intervention scheduling, or the intrinsic resolution used in numerical implementation. Unlike the continuous-time model, variations in h may qualitatively influence the system dynamics. In particular, large values of h can induce discrete-time specific phenomena such as period-doubling or Neimark–Sacker bifurcations. Therefore, bifurcations with respect to h should be interpreted as intrinsic effects of temporal discretization rather than direct biological transitions. The initial conditions satisfy

$$x_0 > 0, \quad y_0 > 0, \quad \upsilon_0 > 0, \quad z_0 > 0, \quad w_0 > 0,$$

ensuring the biological feasibility of the discrete trajectories.

3. Existence of Equilibrium Points

The basic reproduction number, denoted by $\mathcal{R}_0$, plays a fundamental role in determining whether the viral infection can invade and persist within the tumor population. Biologically, $\mathcal{R}_0$ represents the expected number of newly infected tumor cells generated by a single infected cell during its infectious lifetime. Using the next-generation matrix approach [17], system (1) can be expressed as

$$\frac{d\chi}{dt} = F(\chi) - V(\chi),$$

where

$$\chi = (x, y, \upsilon, z, w)^T.$$

The new infection terms are given by

$$F(\chi) = \begin{pmatrix} 0 \\ \beta x \upsilon \\ 0 \\ 0 \\ 0 \end{pmatrix}.$$

Evaluating the Jacobian matrices at the virus-free equilibrium

$$E_1 = (k, 0, 0, 0, 0),$$

for the infected compartments (y, υ) yields

$$F = \begin{pmatrix} 0 & 0 \\ \beta k & 0 \end{pmatrix}, \qquad V = \begin{pmatrix} \alpha & 0 \\ -b\alpha & \theta \end{pmatrix}.$$

Consequently,

$$\mathcal{R}_0 = \rho(FV^{-1}) = \frac{\beta k b}{\theta}.$$

If $\mathcal{R}_0 < 1$, the viral infection cannot persist in the tumor population. If $\mathcal{R}_0 > 1$, viral invasion becomes possible.

Equilibrium Points

System (2) admits the following equilibrium points.

(i) The trivial equilibrium:

$$E_0 = (0, 0, 0, 0, 0).$$

(ii) The virus-free equilibrium:

$$E_1 = (k, 0, 0, 0, 0).$$

(iii) The tumor–immune equilibrium (absence of virus):

$$E_2 = \left(\frac{\delta_1}{\gamma_3},\, 0,\, 0,\, \frac{r}{\gamma_1}\left(1 - \frac{\delta_1}{k\gamma_3}\right),\, 0 \right),$$

which exists whenever

$$\frac{\delta_1}{\gamma_3} < k.$$

(iv) The virus-only equilibrium (no immune response):

$$E_3 = \left(\frac{\theta}{b\beta},\, \frac{\theta}{\alpha b}\upsilon_3^*,\, \upsilon_3^*,\, 0,\, 0 \right),$$

where

$$\upsilon_3^* = \frac{r\theta}{bk\beta^2}(\mathcal{R}_0 - 1).$$

Thus, E_3 exists if and only if $\mathcal{R}_0 > 1$.

(v) The virus-specific immune equilibrium ($z = 0$):

$$E_4 = (x_4^*, y_4^*, \upsilon_4^*, 0, w_4^*),$$

with

$$y_4^* = \frac{\delta_2}{\gamma_5}, \qquad \upsilon_4^* = \frac{b\alpha\delta_2}{\theta\gamma_5},$$

$$x_4^* = k\left(1 - \frac{\alpha b\beta\delta_2}{r\theta\gamma_5}\right), \qquad w_4^* = \frac{\alpha}{\gamma_2}\left(\frac{\beta b}{\theta}x_4^* - 1\right).$$

This equilibrium exists in the positive orthant provided

$$\beta < \frac{r\theta\gamma_5}{\alpha b\delta_2}, \qquad \frac{\beta b}{\theta}x_4^* > 1.$$

(vi) The tumor-specific immune equilibrium ($w = 0$):

$$E_5 = (x_5^*, y_5^*, \upsilon_5^*, z_5^*, 0),$$

where

$$\gamma_3 x_5^* + \gamma_4 y_5^* = \delta_1, \qquad \upsilon_5^* = \frac{b\alpha}{\theta}y_5^*,$$

$$\gamma_1 z_5^* = r\left(1 - \frac{x_5^*}{k}\right) - \beta\upsilon_5^*, \qquad \beta x_5^*\upsilon_5^* = y_5^*(\gamma_1 z_5^* + \alpha).$$

Existence requires positivity of all components.

(vii) The coexistence equilibrium:

$$E_6 = (x_6^*, y_6^*, \upsilon_6^*, z_6^*, w_6^*),$$

where

$$x_6^* = \frac{\delta_1\gamma_5 - \delta_2\gamma_4}{\gamma_3\gamma_5}, \qquad y_6^* = \frac{\delta_2}{\gamma_5}, \qquad \upsilon_6^* = \frac{b\alpha\delta_2}{\theta\gamma_5},$$

$$z_6^* = \frac{1}{k\gamma_1}(rk - rx_6^* - k\beta\upsilon_6^*),$$

$$w_6^* = \frac{1}{\gamma_2}\left[\beta\left(1 + \frac{\gamma_4}{\gamma_3}\right) + \frac{rx_6^*}{k} + \frac{\alpha b\beta\delta_1}{\theta\gamma_3} - \alpha - r\right].$$

Lemma 1. *Assume all parameters are positive. The coexistence equilibrium E_6 exists in the positive orthant if*

$$\delta_1\gamma_5 > \delta_2\gamma_4, \qquad \frac{x_6^*}{k} + \frac{\beta\upsilon_6^*}{r} < 1,$$

$$\beta\left(1 + \frac{\gamma_4}{\gamma_3}\right) + \frac{rx_6^*}{k} + \frac{\alpha b\beta\delta_1}{\theta\gamma_3} > \alpha + r.$$

4. Stability of Equilibria

In this section, we investigate the local stability of the equilibrium points of the discrete model (2).

Theorem 1. *For system (2), the following statements hold:*

(i) The trivial equilibrium point E_0 is unstable.

(ii) If $\mathcal{R}_0 < 1$, then the virus-free equilibrium E_1 is asymptotically stable if and only if

$$h < \min\left\{\frac{2}{\delta_2}, \frac{2}{r}, \frac{2}{\delta_1 - k\gamma_3}, \frac{2}{\chi_+}, \frac{2}{\chi_-}\right\}.$$

Proof.

(i) The Jacobian matrix evaluated at E_0 is

$$J(E_0) = \begin{bmatrix} 1+rh & 0 & 0 & 0 & 0 \\ 0 & 1-\alpha h & 0 & 0 & 0 \\ 0 & 0 & 1-\theta h & 0 & 0 \\ 0 & 0 & 0 & 1-\delta_1 h & 0 \\ 0 & 0 & 0 & 0 & 1-\delta_2 h \end{bmatrix}. \tag{3}$$

Its eigenvalues are

$$\lambda_1 = 1+rh, \quad \lambda_2 = 1-\alpha h, \quad \lambda_3 = 1-\theta h, \quad \lambda_4 = 1-\delta_1 h, \quad \lambda_5 = 1-\delta_2 h.$$

Since $r > 0$ and $h > 0$, we have $\lambda_1 > 1$, hence E_0 is unstable.

(ii) The Jacobian matrix evaluated at E_1 is

$$J(E_1) = \begin{bmatrix} 1-rh & 0 & -k\beta h & -k\gamma_1 h & 0 \\ 0 & 1-\alpha h & k\beta h & 0 & 0 \\ 0 & \alpha b h & 1-\theta h & 0 & 0 \\ 0 & 0 & 0 & 1-h(\delta_1 - k\gamma_3) & 0 \\ 0 & 0 & 0 & 0 & 1-\delta_2 h \end{bmatrix}. \tag{4}$$

The eigenvalues are

$$\lambda_1 = 1-\delta_2 h, \quad \lambda_2 = 1-rh, \quad \lambda_3 = 1-h(\delta_1 - k\gamma_3),$$

$$\lambda_{4,5} = 1 - h\chi_{\pm},$$

where

$$\chi_{\pm} = \frac{1}{2}\left(\alpha + \theta \pm \sqrt{(\alpha-\theta)^2 + 4\alpha b k \beta}\right).$$

When $\mathcal{R}_0 < 1$, it follows that $\chi_- > 0$. The condition $|\lambda_i| < 1$ for all $i = 1, \ldots, 5$ yields

$$|\lambda_1| < 1 \iff h < \frac{2}{\delta_2},$$

$$|\lambda_2| < 1 \iff h < \frac{2}{r},$$

$$|\lambda_3| < 1 \iff h < \frac{2}{\delta_1 - k\gamma_3},$$

$$|\lambda_{4,5}| < 1 \iff h < \frac{2}{\chi_{\pm}}.$$

Therefore, E_1 is asymptotically stable if and only if

$$h < \min\left\{\frac{2}{\delta_2}, \frac{2}{r}, \frac{2}{\delta_1 - k\gamma_3}, \frac{2}{\chi_+}, \frac{2}{\chi_-}\right\}.$$

□

Consider now the general nonlinear discrete-time system

$$x_{i+1} = f_\mu(x_i), \tag{5}$$

where $x_i \in \mathbb{R}^n$ and $\mu \in \mathbb{R}^m$ is a parameter vector. Let the characteristic polynomial of the Jacobian matrix at an equilibrium point x_0 be

$$F_\mu(\lambda) = a_0(\mu)\lambda^n + a_1(\mu)\lambda^{n-1} + \cdots + a_n(\mu).$$

The equilibrium x_0 is asymptotically stable if and only if all eigenvalues of the Jacobian matrix lie strictly inside the unit circle.

Theorem 2. *[16] The characteristic polynomial $F(\lambda)$ has all its roots inside the unit circle if and only if*

(a) $F(1) > 0$ and $(-1)^n F(-1) > 0$,

(b) $\Delta_1^{\pm} > 0, \Delta_3^{\pm} > 0, \ldots, \Delta_{n-1}^{\pm} > 0$ (when n is even), or $\Delta_2^{\pm} > 0, \Delta_4^{\pm} > 0, \ldots, \Delta_{n-1}^{\pm} > 0$ (when n is odd).

The quantities $\Delta_i^{\pm}$ denote the Schur–Cohn determinants associated with the characteristic polynomial $F(\lambda)$ and provide algebraic criteria for determining whether all eigenvalues lie strictly inside the unit circle. They are defined as

$$\Delta_i^{\pm} = |A_i \pm B_i|, \tag{6}$$

where the matrices A_i and B_i are constructed recursively from the coefficients $a_0, a_1, \ldots, a_n$ of $F(\lambda)$ according to the classical Schur–Cohn procedure (see, e.g., [18, 19]).

More precisely, A_i and B_i are formed from structured Toeplitz-type matrices generated by the coefficient vector $(a_0, a_1, \ldots, a_n)$ and its reversed sequence, and $\Delta_i^{\pm}$ correspond to the associated principal minors. The positivity of these determinants guarantees that all roots of $F(\lambda)$ lies inside the unit circle, thereby ensuring local asymptotic stability of the equilibrium in the discrete-time system.

For model (2), the stability of E_i^*, $i = 2, 3, 4, 5$, can be examined as follows.

Proposition 1. *Let*

$$F(\lambda) = \lambda^5 + a_1\lambda^4 + a_2\lambda^3 + a_3\lambda^2 + a_4\lambda + a_5 \tag{7}$$

be the characteristic polynomial of $J(E_i^*)$.

The Jacobian matrix at E_i^* is

$$J(E_i^*) = \begin{bmatrix} 1-\zeta_1 h & 0 & -\beta h x_i^* & -\gamma_1 h x_i^* & 0 \\ \beta h v_i^* & 1-\zeta_2 h & \beta h x_i^* & -\gamma_1 h y_i^* & -\gamma_2 h y_i^* \\ 0 & \alpha b h & 1-\theta h & 0 & 0 \\ \gamma_3 h z_i^* & \gamma_4 h z_i^* & 0 & 1-\zeta_3 h & 0 \\ 0 & \gamma_5 h w_i^* & 0 & 0 & 1-\zeta_4 h \end{bmatrix}, \tag{8}$$

where

$$\zeta_1 = \beta v_i^* + \gamma_1 z_i^* + r\left(\frac{2x_i^*}{k} - 1\right),$$
$$\zeta_2 = \alpha + \gamma_2 w_i^* + \gamma_1 z_i^*,$$
$$\zeta_3 = \delta_1 - \gamma_3 x_i^* - \gamma_4 y_i^*,$$
$$\zeta_4 = \delta_2 - \gamma_5 y_i^*.$$

Applying Theorem 2, E_i^* is asymptotically stable if and only if the Schur–Cohn conditions hold:

$$\begin{cases} F(1) > 0, \\ F(-1) < 0, \\ \Delta_2^{\pm} > 0, \\ \Delta_4^{+} > 0, \\ \Delta_4^{-} > 0. \end{cases} \tag{9}$$

Otherwise, E_i^* is unstable.

The preceding analysis shows that the local behavior of equilibrium points depends on the location of the eigenvalues of the Jacobian matrix relative to the unit circle. In discrete-time systems, qualitative changes occur when one or more eigenvalues cross the unit circle as parameters vary. Such crossings may lead to different types of bifurcations. In the following section, we investigate how variations in the time step size and infection rate may induce flip, fold, or Neimark–Sacker bifurcations in the proposed model.

5. Bifurcations

This section investigates codimension-one bifurcations of the discrete model (2). Bifurcation analysis provides a rigorous framework for explaining qualitative changes in system dynamics caused by small variations in key parameters. In discrete-time tumor–virus–immune interactions, such transitions may correspond to switching between steady tumor control, sustained oscillations, or more complex temporal patterns.

Here, we focus on two parameters of primary interest: the time step size h and the infection rate β. The time step size is intrinsic to the discrete formulation (and may also reflect the resolution of observation or intervention), while β represents the strength of virus-mediated infection of tumor cells. We derive algebraic conditions for the existence of three codimension-one bifurcations: flip (period-doubling), fold, and Neimark–Sacker (N–S) bifurcations of model (2).

5.1. Flip bifurcation

A flip bifurcation (also called a period-doubling bifurcation) occurs when an equilibrium loses stability through a real eigenvalue crossing -1, giving rise to a period-two orbit. Since eigenvalues are evaluated relative to the unit circle, this phenomenon is specific to nonlinear discrete-time systems. Moreover, repeated period-doubling bifurcations may lead to complex dynamics, including chaotic behavior.

Let $J(\mu_0, x_0)$ denote the Jacobian matrix of system (5) evaluated at an equilibrium point x_0, where μ_0 is a bifurcation parameter. At a flip bifurcation, exactly one eigenvalue satisfies $\lambda = -1$ while all remaining eigenvalues lie strictly inside the unit circle. An algebraic criterion for detecting flip bifurcations in discrete-time dynamical systems was established in [20].

Theorem 3. *[20] For a general n-dimension system (5), a flip bifurcation occurs at the parameter $\mu = \mu_0$ if the following conditions are satisfied:*

($\mathbf{C}_{11}$) *(Eigenvalue assignment)*
$F_{\mu_0}(-1) = 0$, $F_{\mu_0}(1) > 0$, $\Delta^{\pm}_{n-1}(\mu_0) > 0$ *and* $\Delta^{\pm}_{j}(\mu_0) > 0$, $j = n-3, n-5, \ldots$.
($\mathbf{C}_{12}$) *(Transversality condition)*
$\dfrac{d}{d\mu} F_{\mu}(-1)\Big|_{\mu=\mu_0} \neq 0.$

Condition ($\mathbf{C}_{11}$) ensures that one real eigenvalue of $J(\mu_0, x_0)$ lies on the unit circle at $\lambda = -1$ while the remaining eigenvalues are strictly inside the unit circle. Condition ($\mathbf{C}_{12}$) guarantees transversality, meaning that the critical eigenvalue crosses the unit circle with nonzero speed as the bifurcation parameter varies.

Applying Theorem 3, we derive the flip bifurcation conditions for model (2) at the coexistence equilibrium E_6 when the step size h is taken as the bifurcation parameter. Specifically, model (2) may undergo a flip bifurcation at E_6 if the following semi-algebraic system holds:

$$\begin{cases} e_1 : -1 + a_1 - a_2 + a_3 - a_4 + a_5 = 0, \\ e_2 : 1 + a_1 + a_2 + a_3 + a_4 + a_5 > 0, \\ e_3 : \Delta_4^- > 0, \\ e_4 : \Delta_4^+ > 0, \\ e_5 : \Delta_2^{\pm} > 0, \\ e_6 : \dfrac{\partial}{\partial h}\left(-1 + a_1 - a_2 + a_3 - a_4 + a_5\right) \neq 0, \\ e_7 : 5 - 4a_1 + 3a_2 - 2a_3 + a_4 \neq 0. \end{cases} \tag{10}$$

A flip bifurcation occurs if there exists at least one real solution satisfying system (10) for some value of h. From a modeling perspective, this transition indicates a loss of equilibrium stability and the emergence of alternating dynamics with period two. In the tumor–virus–immune setting, such oscillations may be interpreted as recurrent fluctuations in tumor burden and immune activity driven by the discrete interaction structure and parameter values, rather than convergence to a steady outcome.

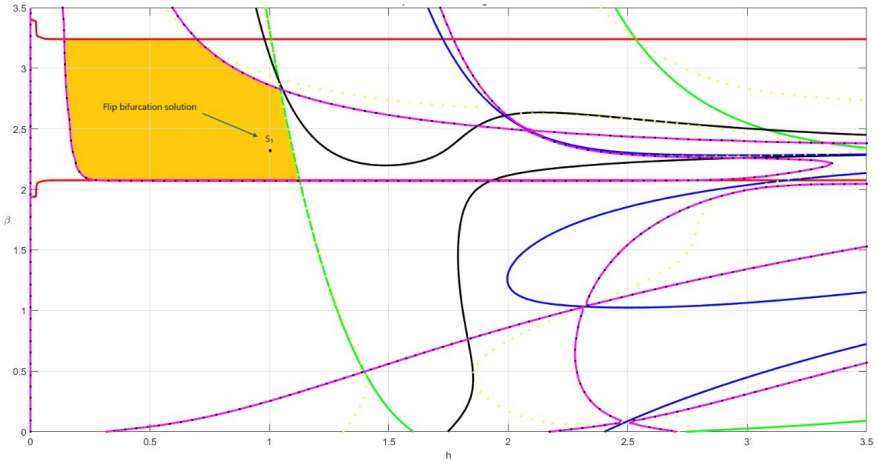

Figure 2: Flip bifurcation diagram for model (2) w.r.t. the parameter h when $r = 3.09$, $k = 1.02$, $\alpha = 0.26$, $b = 0.9$, $\theta = 0.729$, $\delta_1 = 0.7$, $\delta_2 = 0.8$, $\gamma_1 = 0.9$, $\gamma_2 = 0.8$, $\gamma_3 = 0.85$, $\gamma_4 = 0.1$, $\gamma_5 = 0.7$, and $\beta = 2.32$.

Figure 2 illustrates the solution set of the semi-algebraic system (10). The shaded region indicates the parameter domain in which the inequality constraints are simultaneously satisfied, whereas the blank region corresponds to parameter values for which these inequalities fail to admit a real solution. The black curve represents the equality condition e_1 (corresponding to the eigenvalue crossing at -1), while the yellow curves correspond to the remaining nondegeneracy constraints. According to Theorem 3, a flip bifurcation point occurs where the equality curve intersects the admissible region.

5.2. Fold bifurcation

A fold (saddle–node) bifurcation is a codimension-one local bifurcation in which two equilibrium points collide and either disappear or are created as a bifurcation parameter varies. In discrete-time systems, this phenomenon occurs when a real eigenvalue crosses $+1$ while all remaining eigenvalues remain strictly inside the unit circle.

In the proposed tumor–virus–immune model, we take the infection rate β as the bifurcation parameter. Since β governs the strength of virus-mediated infection of tumor cells, it plays a central role in determining whether viral invasion can alter the qualitative structure of the equilibrium states.

Theorem 4. *[20] For a general n-dimension system (5), a fold bifurcation occurs at $\mu = \mu_0$ if the following conditions are satisfied:*

($\mathbf{C_{21}}$) *(Eigenvalue assignment)*
$F_{\mu_0}(1) = 0$, $(-1)^n F_{\mu_0}(-1) > 0$, $\Delta^{\pm}_{n-1}(\mu_0) > 0$ *and* $\Delta^{\pm}_{j}(\mu_0) > 0$, $j = n-3, n-5, \ldots$.
($\mathbf{C_{22}}$) *(Transversality condition)*
$\dfrac{d}{d\mu} F_\mu(1)\Big|_{\mu=\mu_0} \neq 0.$

Applying Theorem 4 to model (2) at the coexistence equilibrium E_6 and taking β as the bifurcation parameter, we obtain the following semi-algebraic system:

$$\begin{cases} f_1 : 1 + a_1 + a_2 + a_3 + a_4 + a_5 = 0, \\ f_2 : -1 + a_1 - a_2 + a_3 - a_4 + a_5 < 0, \\ f_3 : \Delta_4^- > 0, \\ f_4 : \Delta_4^+ > 0, \\ f_5 : \Delta_2^{\pm} > 0, \\ f_6 : \dfrac{\partial}{\partial \beta}\left(1 + a_1 + a_2 + a_3 + a_4 + a_5\right) \neq 0. \end{cases} \tag{11}$$

A fold bifurcation occurs if there exists at least one real solution satisfying system (11) for some value of β. In the tumor–virus–immune context, this bifurcation indicates a threshold phenomenon with respect to viral infectivity: when β crosses a critical value, the system may abruptly switch between qualitatively distinct long-term regimes. Therefore, parameter regions near the fold boundary are sensitive in the sense that small variations in β may produce significant changes in the asymptotic tumor–virus–immune interaction dynamics.

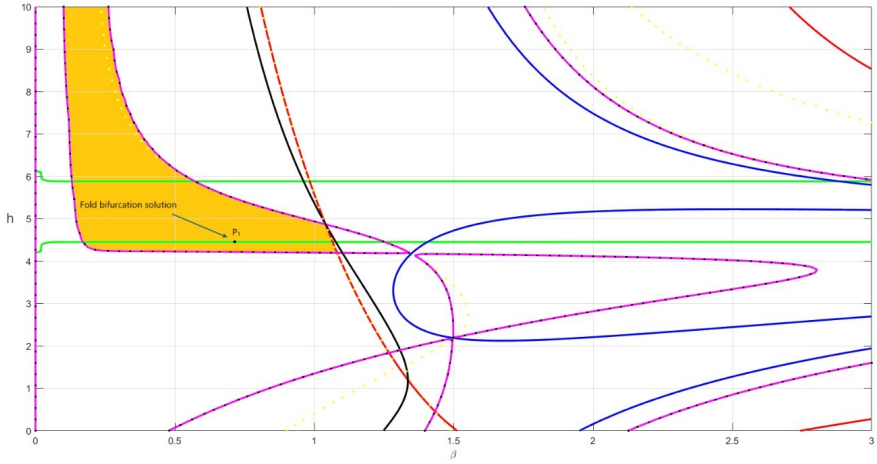

Figure 3: Fold bifurcation diagram for model (2) w.r.t. β when $r = 3.7$, $k = 0.9$, $\alpha = 0.26$, $b = 0.9$, $\theta = 0.729$, $\delta_1 = 0.7$, $\delta_2 = 0.8$, $\gamma_1 = 0.9$, $\gamma_2 = 0.8$, $\gamma_3 = 0.85$, $\gamma_4 = 0$, $\gamma_5 = 0.7$, and $h = 0.7$.

Figure 3 illustrates the solution set of the semi-algebraic system (11). The shaded region represents the admissible parameter domain where all inequality constraints are satisfied, whereas the blank region corresponds to parameter values for which the system does not admit a real solution. The black curve represents the equality condition f_1 (corresponding to the eigenvalue crossing at $+1$). According to Theorem 4, a fold bifurcation point occurs where the equality curve intersects the admissible region.

5.3. Neimark–Sacker bifurcation

The Neimark–Sacker (N–S) bifurcation in discrete-time systems is the counterpart of the Hopf bifurcation in continuous-time systems. It describes a transition from a stable equilibrium to quasi-periodic oscillations on an invariant closed curve (invariant circle). This mechanism plays a fundamental role in generating persistent oscillatory dynamics in nonlinear maps.

Theorem 5. *[21, 22] For a general n-dimensional system (5), a Neimark–Sacker bifurcation occurs at the bifurcation parameter $\mu = \mu_0$ if and only if the following conditions are satisfied:*

(**C$_{31}$**) *(Eigenvalue assignment)*

$$\Delta_{n-1}^{-}(\mu_0) = 0, \quad (-1)^n F_{\mu_0}(-1) > 0, \quad F_{\mu_0}(1) > 0, \quad \Delta_{n-1}^{+}(\mu_0) > 0,$$

and

$$\Delta_j^{\pm}(\mu_0) > 0, \quad j = n-3, n-5, \ldots$$

(**C$_{32}$**) *(Transversality condition)*

$$\frac{d}{d\mu}\Delta_{n-1}^{-}(\mu)\Big|_{\mu=\mu_0} \neq 0.$$

(**C$_{33}$**) *(Nonresonance condition)*

$$\cos\left(\frac{2\pi}{m}\right) \neq 1 - \frac{F_{\mu_0}(1)\Delta_{n-3}^{-}(\mu_0)}{2\Delta_{n-2}^{+}(\mu_0)}, \quad m = 3, 4, 5, \ldots.$$

In the present study, Theorem 5 is applied to the discrete bladder cancer model (2). We take the time step size h as the bifurcation parameter. This choice is natural in discrete-time models since varying h may induce qualitative changes in the dynamics even when the underlying continuous-time system remains stable.

From a dynamical viewpoint, an N–S bifurcation occurs when a pair of complex conjugate eigenvalues of the Jacobian matrix at an equilibrium point crosses the unit circle while all remaining eigenvalues remain strictly inside. In the tumor–virus–immune setting, this transition corresponds to the loss of equilibrium stability through oscillatory modes. The resulting dynamics may exhibit quasi-periodic oscillations reflecting sustained interaction cycles among tumor cells, virus particles, and immune responses. These oscillations should be interpreted as qualitative regimes of the model rather than direct clinical predictions.

Applying Theorem 5 to model (2) at the coexistence equilibrium E_6 and taking h as the bifurcation parameter, we obtain the following semi-algebraic system characterizing

the N–S bifurcation:

$$\begin{cases} \Delta_4^- = 0, \\ F(1) = 1 + a_1 + a_2 + a_3 + a_4 + a_5 > 0, \\ F(-1) = -1 + a_1 - a_2 + a_3 - a_4 + a_5 < 0, \\ \Delta_2^{\pm} \equiv \mp a_1 a_5 - a_5^2 \pm a_4 + 1 > 0, \\ \Delta_4^+ > 0, \\ \dfrac{\partial}{\partial h}\Delta_4^- \neq 0. \end{cases} \tag{12}$$

A Neimark–Sacker bifurcation occurs if there exists at least one real value of h satisfying system (12). The equality condition $\Delta_4^- = 0$ corresponds to a complex conjugate pair of eigenvalues lying on the unit circle, while the inequalities ensure that the remaining eigenvalues stay strictly inside and that the bifurcation is nondegenerate.

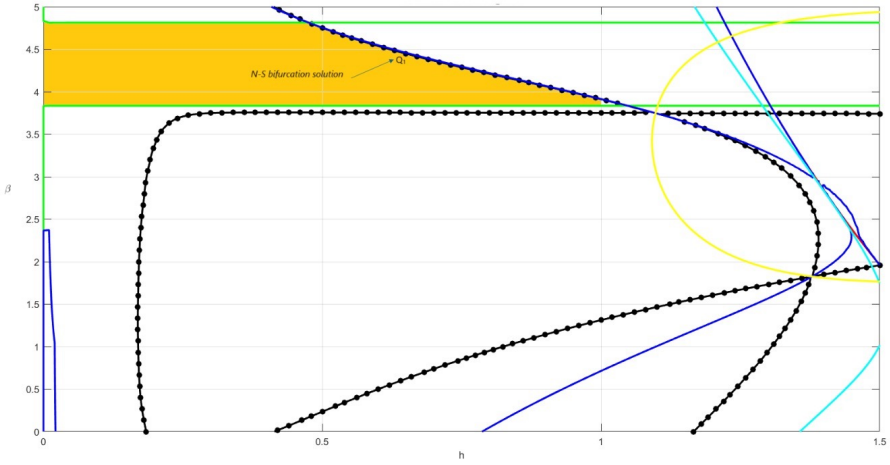

Figure 4: N–S bifurcation diagram for model (2) with respect to h when $r = 3.09$, $k = 1.02$, $\beta = 2.32$, $\alpha = 0.26$, $b = 0.9$, $\theta = 0.729$, $\delta_1 = 0.7$, $\delta_2 = 0.8$, $\gamma_1 = 0.9$, $\gamma_2 = 0.8$, $\gamma_3 = 0.85$, $\gamma_4 = 0.1$, and $\gamma_5 = 0.7$.

Figure 4 illustrates the solution set of the semi-algebraic system (12). The shaded region represents the admissible parameter domain where all inequality constraints are satisfied, whereas the blank region corresponds to parameter values for which the constraints fail to hold simultaneously. The dotted black curve represents the boundary condition $\Delta_4^- = 0$, while the dotted yellow curve represents the remaining nondegeneracy requirement (transversality) $\frac{\partial}{\partial h}\Delta_4^- \neq 0$. According to Theorem 5, an N–S bifurcation point occurs where the boundary curve $\Delta_4^- = 0$ lies within the admissible shaded region, indicating loss of stability of E_6 through a complex conjugate pair of eigenvalues crossing the unit circle.

6. Numerical simulation

In this section, we present numerical simulations to complement the theoretical results established in the previous sections. Simulations were carried out in Maplesoft (2023) to solve the semi-algebraic bifurcation conditions, and in MATLAB R2024a to generate the bifurcation diagrams and phase portraits. We consider three representative numerical examples corresponding to the flip, fold, and Neimark–Sacker bifurcations. The step size h and the infection rate β are selected as the main bifurcation parameters.

Example 1 (Flip bifurcation with respect to h). Let $r = 3.09$, $k = 1.02$, $\alpha = 0.26$, $b = 0.9$, $\theta = 0.729$, $\delta_1 = 0.7$, $\delta_2 = 0.8$, $\gamma_1 = 0.9$, $\gamma_2 = 0.8$, $\gamma_3 = 0.85$, $\gamma_4 = 0.1$, and $\gamma_5 = 0.7$. Solving the flip semi-algebraic system (10) (in Maplesoft 2023) with respect to (h, β) yields an approximate solution $S_1 : (h \approx 1,\ \beta \approx 2.32)$. For these parameter values, model (2) admits a positive coexistence equilibrium

$$E_6 \approx (0.6,\ 1.1,\ 0.3,\ 0.1,\ 0.1).$$

Fixing $\beta = 2.32$ and varying $h \in (0, 1.09)$ with step size 0.001 in MATLAB R2024a produces the flip bifurcation diagram shown in Fig. 5.

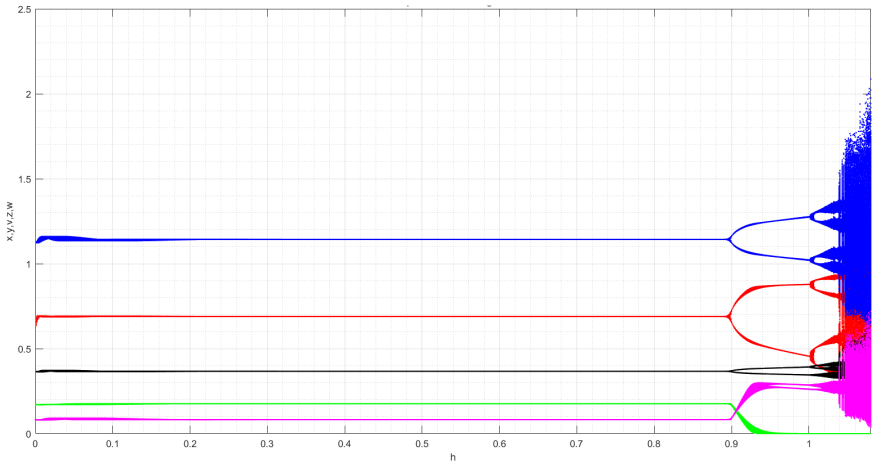

Figure 5: Flip bifurcation diagram of model (2) with respect to h (Example 1).

Figure 5 indicates that the coexistence equilibrium is stable for small step sizes (approximately $h < 0.9$), where trajectories converge to a single steady state. As h increases, the equilibrium loses stability through a period-doubling mechanism, and oscillatory behavior emerges. The subsequent branching structure suggests a cascade of period-doubling bifurcations as the discrete step size increases.

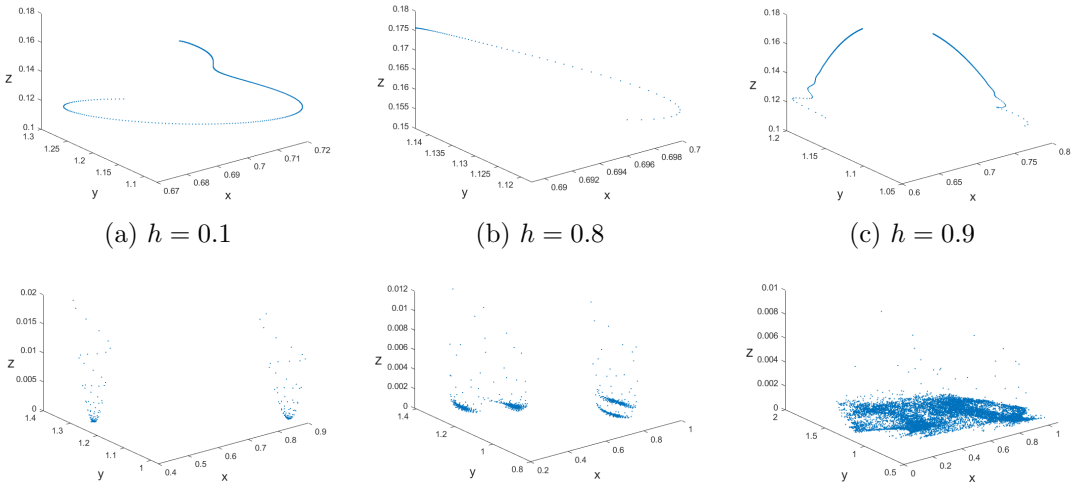

(a) $h = 0.1$ (b) $h = 0.8$ (c) $h = 0.9$

(d) $h = 1$ (e) $h = 1.03$ (f) $h = 1.07$

Figure 6: Phase portraits for varying h corresponding to Fig. 5 (Example 1).

The phase portraits in Fig. 6 further illustrate this transition. For $h < 0.9$ (Fig. 6a–b), trajectories approach a stable fixed point, indicating convergence to a steady tumor–virus–immune coexistence state. Near the critical region (Fig. 6c–d), a stable periodic orbit appears, reflecting sustained oscillations among the interacting populations. For larger values (Fig. 6e–f), the oscillations become more complex, indicating increased sensitivity of the discrete dynamics to the step size.

Example 2 (Fold bifurcation with respect to β). In this example, β represents the infection rate of tumor cells by the virus and therefore directly controls the strength of virus-mediated tumor infection. Let $r = 3.7$, $k = 0.9$, and keep the remaining parameters as in Example 1. Solving the *fold* semi-algebraic system (11) in the (h, β)-plane yields an approximate solution $P_1 : (h \approx 0.7,\ \beta \approx 4.45)$. For these parameter values, model (2) has a coexistence equilibrium

$$E_6 \approx (0.36,\ 1.1,\ 0.36,\ 0.37,\ 1.4 \times 10^{-7}).$$

Fixing $h = 0.7$ and varying $\beta \in (1, 5)$ produces the fold bifurcation diagram in Fig. 7.

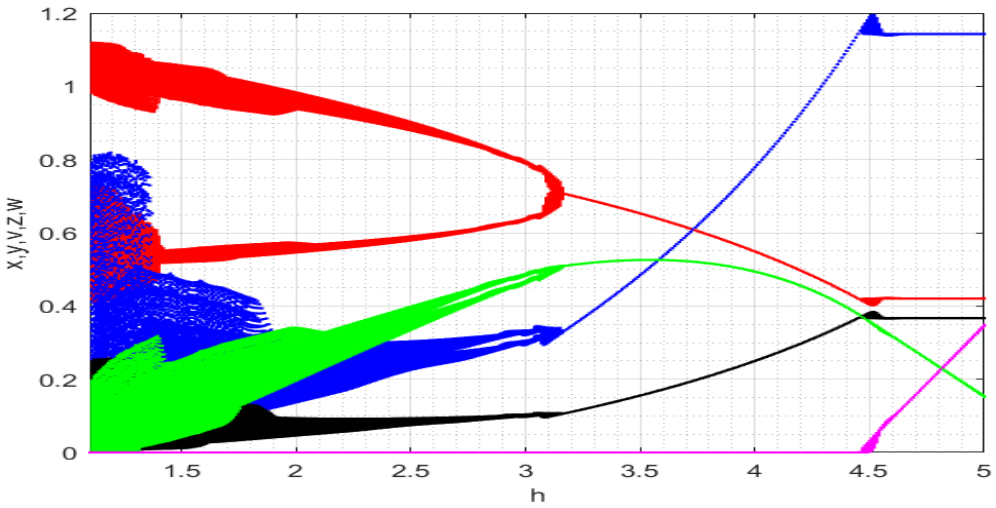

Figure 7: Fold bifurcation diagram of model (2) with respect to β (Example 2).

Figure 7 shows a qualitative transition in the equilibrium structure as β increases. For smaller infection rates, the observed dynamics are more irregular and may exhibit oscillatory patterns. Near the critical value, a fold bifurcation occurs, meaning that two equilibrium branches collide and one branch disappears. For sufficiently large β, the system evolves toward a single stable equilibrium configuration.

From a biological standpoint, increasing β strengthens virus–tumor contact and accelerates conversion of uninfected tumor cells into infected cells. The fold bifurcation therefore identifies a threshold in viral infectivity at which the long-term behavior of the tumor–virus–immune interaction changes qualitatively. This should be interpreted as a dynamical regime shift rather than a direct guarantee of tumor elimination.

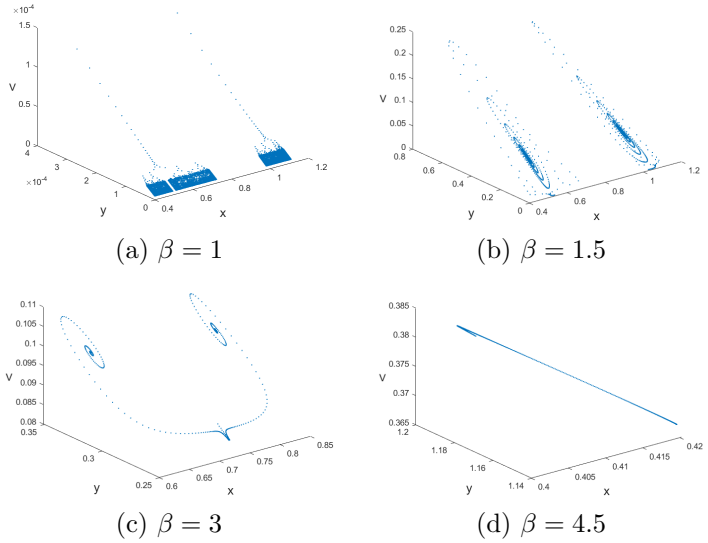

(a) $\beta = 1$ (b) $\beta = 1.5$

(c) $\beta = 3$ (d) $\beta = 4.5$

Figure 8: Phase portraits of model (2) for selected values of β corresponding to Fig. 7 (Example 2).

The phase portraits in Fig. 8 show how trajectories evolve as β changes. For $\beta = 1$ (Fig. 8a), trajectories are widely scattered, suggesting nonconvergent behavior and strong fluctuations. At $\beta = 1.5$ (Fig. 8b), closed orbits emerge, indicating sustained periodic oscillations. At $\beta = 3$ (Fig. 8c), the phase-space structure becomes more complex, consistent with coexistence of oscillatory regimes. For $\beta = 4.5$ (Fig. 8d), trajectories collapse toward a steady-state configuration, consistent with stabilization after the fold transition.

Example 3 (Neimark–Sacker bifurcation with respect to h). Let $r = 2.5$, $k = 1.1$, $\alpha = 0.25$, $b = 0.85$, $\theta = 0.7$, $\delta_1 = 0.65$, $\delta_2 = 0.75$, $\gamma_1 = 0.88$, $\gamma_2 = 0.75$, $\gamma_3 = 0.8$, $\gamma_4 = 0.28$, and $\gamma_5 = 0.68$. Solving the N–S semi-algebraic system (12) with respect to (h, β) yields an approximate solution $Q_1 : (h \approx 0.975,\ \beta \approx 4.2)$. Accordingly, model (2) admits a positive coexistence equilibrium

$$E_6 \approx (0.34,\ 1.1,\ 0.33,\ 0.26,\ 0.002).$$

Fixing $\beta = 4.2$ and varying $h \in (0.8, 1.15)$ produces the N–S bifurcation diagram shown in Fig. 9.

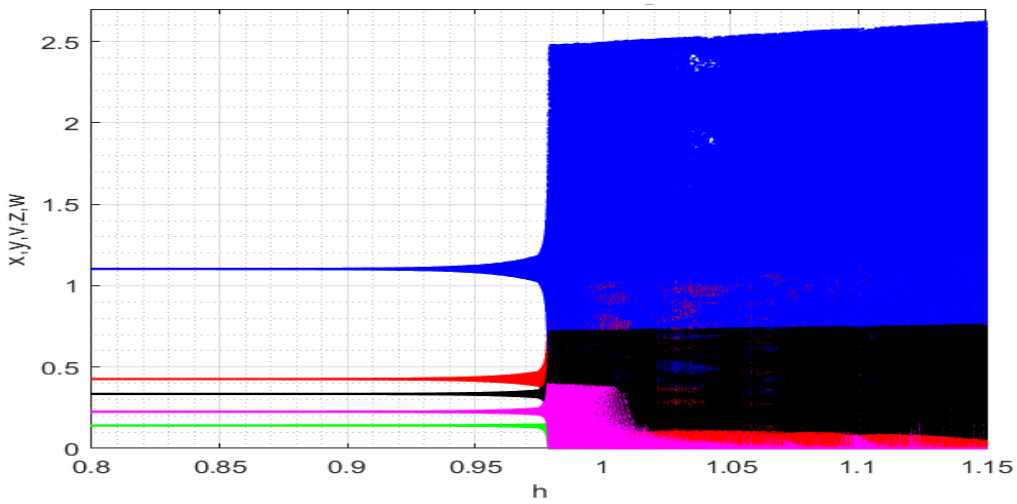

Figure 9: N–S bifurcation diagram of model (2) with respect to the step size h (Example 3).

Figure 9 suggests that for $0.9 < h < 0.95$ the system converges to a stable equilibrium. Near $h \approx 0.95$, the equilibrium loses stability via a Neimark–Sacker bifurcation, leading to the emergence of oscillatory modes associated with quasi-periodic dynamics. As h increases further, the distribution of points broadens, indicating increasingly complex temporal patterns and stronger sensitivity to the discrete step size.

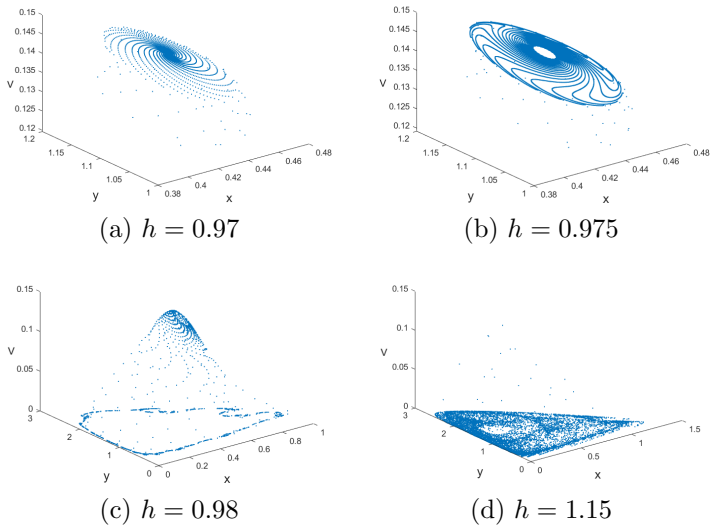

(a) $h = 0.97$ (b) $h = 0.975$

(c) $h = 0.98$ (d) $h = 1.15$

Figure 10: Phase portraits of model (2) for selected h values corresponding to Fig. 9 (Example 3).

The phase portraits in Fig. 10 illustrate the qualitative change of the dynamics across the N–S transition. For $h = 0.97$–0.975 (Fig. 10a–b), trajectories exhibit structured oscillatory motion, consistent with the onset of quasi-periodic behavior following the loss of fixed-point stability. For $h = 0.98$ (Fig. 10c), the phase-space structure becomes less organized, indicating increasing dynamical complexity. For $h = 1.15$ (Fig. 10d), trajectories become highly scattered, consistent with strong irregular fluctuations. These outcomes highlight that the discrete step size may act as a critical driver of stability switching and complex oscillatory dynamics in the proposed discrete tumor–virus–immune model.

7. Conclusion

This work developed and analyzed a discrete-time bladder cancer–immune–virotherapy model describing the interactions among uninfected tumor cells, infected tumor cells, free virus particles, tumor-specific immune cells, and virus-specific immune cells. The discrete model was derived via the forward Euler scheme applied to a biologically motivated continuous framework, which allowed us to examine dynamical behaviors that can be specific to discrete-time updates.

We established existence conditions for biologically meaningful equilibrium points and obtained local stability criteria using algebraic techniques. The basic reproduction number was derived to characterize the viral invasion threshold. The analysis shows that the stability of the interior coexistence equilibrium is strongly influenced by key parameters, particularly the infection rate β and the step size h.

A main contribution of the study is the systematic characterization of codimension-one bifurcations in the discrete setting. In particular, we identified parameter regimes where the model undergoes flip (period-doubling), fold (saddle–node), and Neimark–Sacker bi-

furcations. These bifurcations partition the parameter space into distinct qualitative dynamical regimes: flip bifurcations lead to periodic solutions of higher period, fold bifurcations mark threshold effects associated with the creation or disappearance of equilibria, and Neimark–Sacker bifurcations generate quasi-periodic oscillations on invariant closed curves.

Numerical simulations support the theoretical results and demonstrate how varying β and h can induce transitions between stable steady behavior, sustained oscillations, and more complex temporal patterns. These outcomes highlight the sensitivity of the discrete tumor–virus–immune dynamics to parameter variation and illustrate how temporal discretization may qualitatively alter long-term behavior compared to continuous-time formulations.

Overall, the proposed framework provides a structured approach for studying stability switching and bifurcation mechanisms in discrete tumor virotherapy models. Future work may include parameter estimation and calibration using experimental or clinical data, comparison with the corresponding continuous-time system under matched time scales, and extensions incorporating additional biological components such as treatment scheduling, immune exhaustion, or time delays.

References

[1] P. Dong, A. Mao, W. Qiu, and G. Li. Improvement of cancer prevention and control: reflection on the role of emerging information technologies. *Journal of Medical Internet Research*, 26:e50000, 2024.

[2] A. C. Costa, J. M. Santos, R. M. G. da Costa, and R. Medeiros. Impact of immune cells on the hallmarks of cancer: A literature review. *Critical Reviews in Oncology/Hematology*, 168:103541, 2021.

[3] L. M. van Hoogstraten, A. Vrieling, A. G. van der Heijden, M. Kogevinas, A. Richters, and L. A. Kiemeney. Global trends in the epidemiology of bladder cancer: challenges for public health and clinical practice. *Nature Reviews Clinical Oncology*, 20(5):287–304, 2023.

[4] D. E. Magee, D. C. Cheung, A. E. Hird, P. Chung, P. Warde, C. Catton, and G. S. Kulkarni. Cost of bladder cancer care: a single-center comparison of radical cystectomy and trimodal therapy. *Urology Practice*, 10(4):293–299, 2023.

[5] D. Godlewski, S. Czech, J. Szpara, D. Bartusik-Aebisher, and D. Aebisher. A narrative review of current advances and future changes regarding bladder cancer treatment. *Uro*, 5(2):11, 2025.

[6] F. Del Giudice, V. Asero, E. Bologna, C. M. Scornajenghi, D. Carino, V. Dolci, and E. De Berardinis. Efficacy of different bcg strains on recurrence rates among nmibc. *Cancers*, 15(7):1937, 2023.

[7] R. Ma, Z. Li, E. A. Chiocca, M. A. Caligiuri, and J. Yu. Oncolytic virus-based cancer immunotherapy. *Trends in Cancer*, 9(2):122–139, 2023.

[8] B. Liu, H. Zhou, L. Tan, K. T. H. Siu, and X. Y. Guan. Exploring treatment options in cancer. *Signal Transduction and Targeted Therapy*, 9(1):175, 2024.

[9] T. Azizi. Mathematical modeling of cancer progression. *AppliedMath*, 4(3):1065–1079, 2024.
[10] S. R. Aderyani, R. Saadati, F. R. Aderyani, and O. Tunç. Tumor-immune dynamics via fractional calculus. *Scientific Reports*, 15(1):29094, 2025.
[11] A. I. Khamidullina, Y. E. Abramenko, A. V. Bruter, and V. V. Tatarskiy. Replication stress response in cancer. *International Journal of Molecular Sciences*, 25(2):1263, 2024.
[12] Y. Feng, H. Yang, G. Liang, J. Chen, T. Li, Y. Wang, and C. Ge. Immune checkpoint inhibitors and virotherapy. *Oncology Research*, 33(12):3801, 2025.
[13] A. K. Abbas, A. H. Lichtman, and S. Pillai. *Cellular and Molecular Immunology*. 2023.
[14] M. Wang, B. Rousseau, K. Qiu, G. Huang, Y. Zhang, H. Su, and L. Huang. Killing tumor-associated bacteria. *Nature Biotechnology*, 2023.
[15] L. Xu, H. Sun, N. R. Lemoine, Y. Xuan, and P. Wang. Oncolytic vaccinia virus and cancer immunotherapy. *Frontiers in Immunology*, 14:1324744, 2024.
[16] J. He and D. Wu. Discrete sylvester-conjugate matrix equations. *arXiv preprint arXiv:2411.02333*, 2024.
[17] P. Van den Driessche and J. Watmough. Further notes on the basic reproduction number. In *Mathematical Epidemiology*, pages 159–178. Springer, 2008.
[18] X. Li, C. Mou, W. Niu, and D. Wang. Stability analysis for discrete biological models. *Mathematics in Computer Science*, 5:247–262, 2011.
[19] S. Elaydi. *An Introduction to Difference Equations*. Springer, 3 edition, 2005.
[20] G. Wen, S. Chen, and Q. Jin. Period-doubling bifurcation criterion. *Journal of Sound and Vibration*, 311(1–2):212–223, 2008.
[21] G. Wen. Criterion to identify hopf bifurcations. *Physical Review E*, 72(2):026201, 2005.
[22] Y. A. Kuznetsov. *Elements of Applied Bifurcation Theory*. Springer, 2004.